An Experimental and Numerical Investigation of Crossflow Effects in Two-Phase Displacements

Y. Cinar, SPE, and **K. Jessen,** SPE, Stanford U.; **R. Berenblyum,** SPE, Technical U. of Denmark; and **R. Juanes,** SPE, and **F.M. Orr Jr.,** SPE, Stanford U.

Summary

In this paper, we present flow visualization experiments and numerical simulations that demonstrate the combined effects of viscous and capillary forces and gravity segregation on crossflow that occurs in two-phase displacements in layered porous media.

We report results of a series of immiscible flooding experiments in 2D, two-layered glass bead models. Favorable mobility-ratio imbibition and unfavorable mobility-ratio drainage experiments were performed. We used pre-equilibrated immiscible phases from a ternary isooctane/isopropanol/water system, which allowed control of the interfacial tension (IFT) by varying the isopropanol concentration. Experiments were performed for a wide range of capillary and gravity numbers. The experimental results illustrate the transitions from flow dominated by capillary pressure at high IFT to flow dominated by gravity and viscous forces at low IFT. The experiments also illustrate the complex interplay of capillary, gravity, and viscous forces that controls crossflow. The experimental results confirm that the transition ranges of scaling groups suggested by Zhou et al. (1994) are appropriate/valid.

We report also results of simulations of the displacement experiments by two different numerical techniques: finite-difference and streamline methods. The numerical simulation results agree well with experimental observations when gravity and viscous forces were most important. For capillary-dominated flows, the simulation results are in reasonable agreement with experimental observations.

Introduction

Streamline methods are very efficient numerical techniques for field-scale reservoir simulation, but they are not without limitations. They treat flow along each streamline as independent of adjacent streamlines and therefore do not typically represent crossflow in the simulations. If users of streamline methods are to interpret simulation results reliably, they will need to assess whether any of the mechanisms not modeled in the simulations are important enough to limit the accuracy of the simulations appreciably.

Transfer of fluid in the direction transverse to streamlines can result from diffusion and dispersion, crossflow caused by viscous and capillary forces, and gravity segregation. The scaling of diffusion and dispersion has been investigated in a number of previous studies. If the injected gas is miscible or partially miscible with the oil, diffusion and dispersion mechanisms may play a significant role in the displacement (Mohanty and Johnson 1993; Fayers and Lee 1994; Tchelepi 1994; Jiang and Butler 1994; Burger and Mohanty 1997). In particular, Burger and Mohanty (1997) showed that diffusion through the oil phase can limit mass transfer from oil residing in low-permeability regions. Similar arguments can also apply to other mechanisms of crossflow: viscous and capillary crossflow as well as gravity segregation (Fayers and Lee 1994; Burger and Mohanty 1997; Zapata and Lake 1981; Zhou et al. 1994).

This paper (SPE 90568) was first presented at the 2004 SPE Annual Technical Conference and Exhibition, Houston, 26–29 September, and revised for publication. Original manuscript received for review 25 July 2005. Revised manuscript received 21 October 2005. Paper peer approved 18 November 2005.

Scaling analysis of crossflow mechanisms for displacements in heterogeneous media allows assessment of the relative contributions of each driving force to flow (Tchelepi 1994; Zhou et al. 1994; Shook et al. 1992). Starting from material balance equations and defining them in dimensionless variables, scaling groups can be obtained that determine the regime of flow during displacement. The relevant scaling groups for displacement of oil by water in systems that contain some simple heterogeneity such as layers are the transverse gravity and capillary numbers, which are given by (Tchelepi 1994; Zhou et al. 1994):

$$N_{gv} = \frac{\Delta\rho g L k_{av}}{H v \mu_o}, \quad \ldots\ldots (1)$$

$$N_{cv} = \frac{L p_c^* k_{av}}{H^2 v \mu_o}, \quad \ldots\ldots (2)$$

$$p_c^* = \int_{S_{wc}}^{1-S_{or}} \frac{p_c(S_w)}{(1 - S_{or} - S_{wc})}\, dS, \quad \ldots\ldots (3)$$

$$R_l^2 = \left(\frac{L}{H}\right)^2 \frac{k_{av}}{k_{ah}}, \quad \ldots\ldots (4)$$

and

$$N_B = \frac{N_{gv}}{N_{cv}} = \frac{\Delta\rho g H}{p_c^*}. \quad \ldots\ldots (5)$$

In Eqs. 1 and 2, N_{gv} and N_{cv} are the ratios of characteristic times for fluid to flow in the transverse direction caused by gravity or capillary forces, respectively, to those in the horizontal direction caused by viscous forces, and p_c^* is a characteristic capillary-pressure difference in the direction transverse to the main flow direction. R_l characterizes the relative impacts of vertical and horizontal flow. N_B is the Bond number, which is a ratio of gravity to capillary forces. Using simulation and experimental results presented in the literature, Zhou et al. (1994) reported criteria that delineate when capillary forces dominate displacement performance as well as when gravity or viscous forces do. They defined transitions between different regimes described as gravity-capillary, viscous-capillary, and viscous-gravity equilibrium. **Table 1** summarizes the conditions of the related scaling groups for transitions between the different regions.

Experimental investigations have shown that crossflow effects can be significant in some settings, especially in heterogeneous media where high- and low-permeability zones exist (Richardson and Perkins 1957; Gaucher and Lindley 1960; Ahmed 1984; Dawe et al. 1992; Schechter et al. 1994; Brock and Orr 1991; Firoozabadi 1994; Wylie and Mohanty 1997; Peters et al. 1998; Orr 2004). Early work (Richardson and Perkins 1957; Gaucher and Lindley 1960) examined crossflow effects on the performance of waterflooding in layered models with vertical communication. It was reported that, as the flow rate and mobility ratio decreased, the oil recovery increased considerably. This was mainly because at faster flow rates, the tendency for water to channel through the more permeable layers increased, which results in early breakthrough. It was also reported that the location of the high-permeability layer had a greater effect on oil recovery than the flow rate. Higher recoveries were obtained from the models that had the coarse-sand

TABLE 1—CONDITIONS FOR TRANSITIONS BETWEEN THE DOMINATED REGIONS (ZHOU ET AL. 1994)

Flow Region	Condition
From viscous- to capillary-dominated	$0.2 < \frac{N_{cv}M}{1+M} < 5.0$
From viscous- to gravity-dominated	$0.2 < \frac{N_{gv}M}{1+M} < 5.0$
From capillary- to gravity-dominated	$0.2 < N_B < 5.0$
Viscous-dominated	$\frac{M\left(N_{cv}+N_{gv}\right)}{1+M} << 1.0$

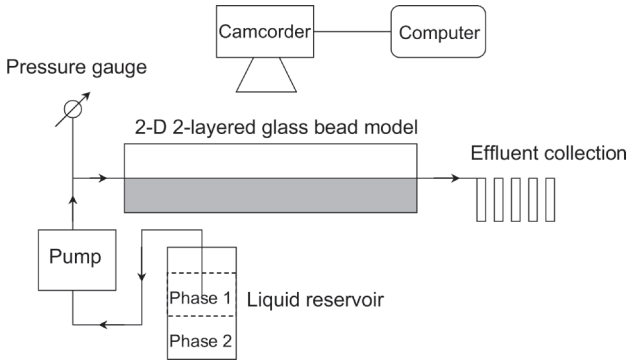

Fig. 1—Schematic of the experimental setup.

layer at the top. Ahmed (1984) reported that crossflow decreased in response to lowering of IFT when emulsion was formed inside the porous system. Dawe et al. (1992) concluded that capillary forces were of greater importance at permeability boundaries. They also observed that the balance between capillary and viscous forces was rate-dependent; the effects of capillary forces became larger as the flow rate decreased. Schechter et al. (1994) reported experiments that demonstrated that imbibition processes changed from capillary-dominated to gravity-dominated when the IFT was lowered from 38.1 to 0.1 mN/m.

Recently, there have been numerous experimental studies that investigated the effects of crossflow driven by viscous and capillary forces and gravity segregation on miscible or near-miscible flooding (Brock and Orr 1991; Firoozabadi 1994; Wylie and Mohanty 1997; Peters et al. 1998). Brock and Orr (1991) reported that viscous fingers in first-contact miscible flooding in homogeneous media occurred by spreading and splitting at their tips, while channeling in heterogeneous media developed along the streamlines that occurred at unit mobility in the same porous media. Firoozabadi (1994) reported experiments that suggest that the first-contact-miscible flooding in fractured media can be a very efficient process because of crossflow between the matrix and the fractures. Burger and Mohanty (1997) and Wylie and Mohanty (1997) presented different types of gas-injection experiments that investigated crossflow-induced mass transfer of oil from bypassed regions to the flowing zones. Their results indicate the following:

1. Orientation of permeability heterogeneities has a significant impact on oil recovery.
2. Mass transfer of oil increases with gas solvent enrichment.
3. Gravity effects can be important, depending on the orientation of the flood.
4. Multiphase flow in near-miscible floods leads to less gravity override compared with the first-contact miscible floods.

Peters et al. (1998) investigated the effects of gravity and viscous forces on crossflow in two-layer experiments. They used brine and water as first-contact miscible fluids. For an experiment with the high-permeability layer on top, they observed that gravity and viscous forces opposed in favorable mobility-ratio experiments (brine displacing water) and acted together in unfavorable mobility-ratio experiments (water displacing brine).

As the theory and experimental observations show, there are multiple combinations and permutations of important physical quantities such as density difference, mobility ratio, orientation of permeability heterogeneity, drainage, and imbibition. Previous research has documented the physical mechanisms for crossflow in heterogeneous systems. This paper provides a systematic set of experiments to quantify the transitions and show that the interplay of capillary, viscous, and gravity forces can be captured by numerical simulation.

Experimental Investigation

Apparatus. Glass beads were used to build a 2D, two-layered flow model. Such models allow the displacement to be directly visible, and they enable control of permeability heterogeneities. A schematic of the experimental setup used in this study is shown in **Fig. 1.**

The glass-bead model was built in the following way. First, glass blocks and fluid-distribution parts were glued together with epoxy to form a box with one side open. PVC was used for fluid-distribution parts and sealing sides of the model. This box was then attached to two pneumatic vibrators. First, small-sized glass beads (Mesh: 60, $d_g \approx 0.021$ cm), and then large glass beads (Mesh: 35, $d_g \approx 0.043$ cm) were dropped into the model under vibration. Water was then let into the model to aid compaction of glass beads, and the packing was pressed firmly by means of a plastic plate. The final piece of the box was then glued in place by applying an additional force on that piece. The water was drained and the model was flushed with dry air for 24 hours. An example of a model is shown in **Fig. 2.** The porosity and permeability of each layer were measured separately using homogeneous packs in a cylindrical tube. The porosity for both layers was approximately 39.5%. The permeabilities of the high-permeability and low-permeability layers were 190 and 52 D, respectively. The average permeabilities of the model in the horizontal and vertical directions are calculated from the individual permeabilities to be 121 and 82 D, respectively. The horizontal permeability of the model was also verified by flow experiments.

The homogeneity of the flow model was checked by a simple experiment. The model was first saturated completely with water. Then, first-contact miscible dyed water was injected into the porous medium. In that flow experiment, the effects of capillary and gravity forces were eliminated. The displacement fronts in each layer should then be determined by the individual layer permeabilities. The images of displacements showed no crossflow and confirmed an acceptable degree of homogeneity of the individual layers [see Orr (2004) for additional details related to these experiments].

The pressure drops across the model and production history were measured during the experiments. The pressure was measured by means of an analog gauge with an accuracy of 0.2 kPa. The effluent fluids were collected in graduated cylinders. After suitable delay for phase separation, the production data were then determined by reading the liquid levels in the cylinders with an accuracy of 0.1 cm^3.

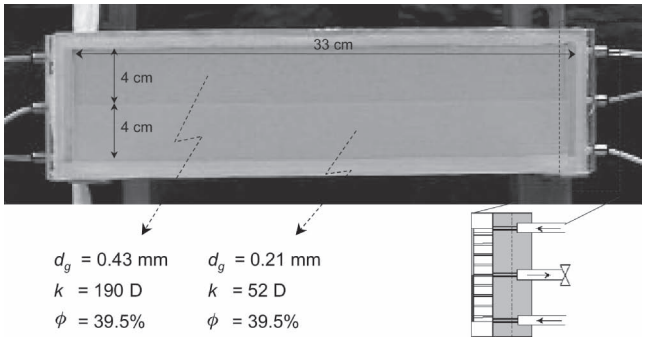

Fig. 2—Glass-bead flow model (width=0.6 cm).

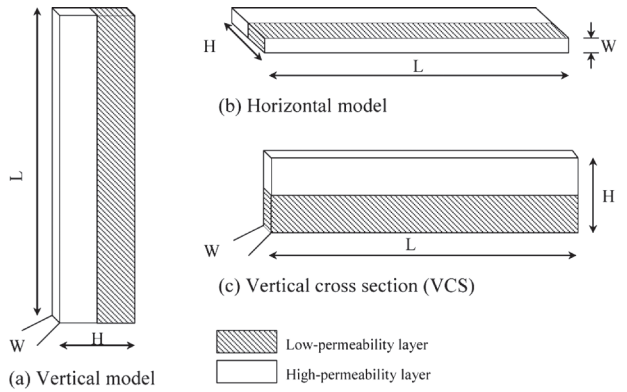

Fig. 3—Orientation of glass-bead models (width=0.6 cm, height=8 cm, and length is given in Table 3).

In the experiments, we systematically changed the orientation of the glass-bead models to investigate different types of crossflow mechanisms. **Fig. 3** shows a sketch of orientations of the glass-bead models used. We reduced the effects of gravity in some experiments by employing vertical displacements (Fig. 3a) and injecting heavier fluid at the bottom of the model to displace lighter fluid, or vice versa. In the vertical displacements, IFT and flow rate determine which of the crossflow mechanisms dominates the displacement. Gravity effects on crossflow in the vertical displacements should be different from those in horizontal displacements depicted in Fig. 3b. To investigate the combined effects of viscous, gravity, and capillary forces on the displacement behavior, we employed displacements in a vertical cross section (VCS) model oriented as shown in Fig. 3c. We also employed similar displacements in long VCS models ($L=53$ cm) to examine the effect of *L/H* on the displacement behavior and in inverted long VCS models with the high-permeability layer at the bottom to investigate the effect of the location of the high-permeability layer, respectively. Results for the short models only are reported here. See Orr (2004) for results of the displacements in the long models.

Fluids. We used two different mixtures from the ternary isooctane (IC_8)/isopropanol (IPA)/water system, in which density, viscosity, and IFT of the phases can be controlled systematically. The first set of phases was a binary mixture of IC_8 and water with a relatively high IFT characteristic of immiscible displacements. The second set was a mixture of all three components (42% IC_8, 11.5% H_2O, and 46.5% IPA by weight), with a much lower IFT representative of near-miscible displacements. The physical properties of the phases are given in **Table 2.** The phases were dyed different colors to track the extent of fluid displacement in the experiments. The effects of using dye in the water-IC_8 solutions on the properties of the phases (i.e., viscosity, density, and IFT) were measured and found to be negligible. In the high-IFT displacements, the water dye did not stay with the water phase, either because the dye partitioned in the oil phase or because it adsorbed onto the glass beads.

Procedure. We employed the following steps to saturate the model initially:

1. Air in the pore space was displaced by CO_2.
2. The CO_2 was displaced by two pore volumes (PV) of dyed IC_8-rich phase or dyed H_2O-rich phase. The "favorable" mobility-ratio "imbibition" displacements were done by injecting the H_2O-rich phase into the IC_8-rich phase-saturated glass bead models, and the "unfavorable" mobility ratio "drainage" displacements were performed by injecting the IC_8-rich phase into the H_2O-rich phase-saturated models.
3. We then injected the dyed H_2O-rich phase (or the dyed IC_8-rich phase). The areas of the model invaded were recorded on video. The pressure drop across the model and the production history were also recorded.

At the beginning of favorable imbibition displacements, we attempted to create an "irreducible" saturation of the H_2O-rich phase in the porous system to represent displacements in actual reservoirs. However, after preliminary test runs, we determined that we could not obtain a reasonably uniform connate saturation of the H_2O-rich phase for the porous system. This was because the injected IC_8-rich phase did not sweep the water-rich phase in the low-permeability layer after breakthrough in the high-permeability layer. In the end, we performed experiments of the H_2O-rich phase displacing the IC_8-rich phase, which saturated the porous medium completely. Therefore, the results obtained from these experiments do not include any effects of connate wetting-phase saturation.

Numerical Modeling

Finite-Difference (FD) Simulation. We used Eclipse 100, a commercial black-oil simulator, to simulate the displacement experiments. We employed a fully implicit scheme with 1,000 gridblocks (100 for length, 10 for height, 1 for width). For high-IFT experiments, the relative-permeability data used in the simulations were obtained for both drainage and imbibition cases from dynamic experiments with IC_8/water systems in uniform glass-bead packs ($\phi=40\%$ and $k=52$ D). Relative permeabilities were estimated using the method of Johnson et al. (1959). The relative-permeability data were smoothed before using them as input in the simulators. For low-IFT displacements, we used near-diagonal relative permeabilities that represent near-miscible floods. We adapted the capillary pressure data presented by Dawe et al. (1992) for various unconsolidated glass-bead packs for an oil/water fluid system to obtain Leverett J-functions (Leverett 1941) for both drainage and imbibition experiments. The data are presented in **Fig. 4.** The capillary-pressure curves were then computed by simple Leverett scaling of the J-function:

$$p_c(S_w)=\frac{\sigma\cos\theta}{\sqrt{k/\phi}}J(S_w), \quad \ldots\ldots\ldots\ldots\ldots\ldots\ldots\ldots\ldots\ldots (6)$$

where σ is the interfacial tension and θ is the contact angle. We used a value of the receding contact angle $\theta_r=0°$ in drainage experiments and a value of the advancing contact angle $\theta_a=45°$ in imbibition experiments (Morrow 1976).

Streamline Simulation. A streamline simulator accounting for capillary and gravity effects (CapSL) was also used to simulate the experiments. The research code, CapSL, is based on the streamline simulator developed by Batycky (1997). In CapSL, capillary and gravity effects are introduced into the pressure and the saturation equations. Introduction of capillary and gravity effects into the pressure equation changes the location of the streamlines. To pre-

TABLE 2—PHYSICAL PROPERTIES OF THE PHASES USED IN THE EXPERIMENTS AT AMBIENT CONDITIONS

	Immiscible		Near-Miscible	
	IC_8-rich	H_2O-rich	IC_8-rich	H_2O-rich
Density (g/cm^3)	0.692	0.998	0.723	0.795
Viscosity (mPa·s)	0.480	1.000	0.836	2.027
IFT (mN/m)	38.0		0.024	

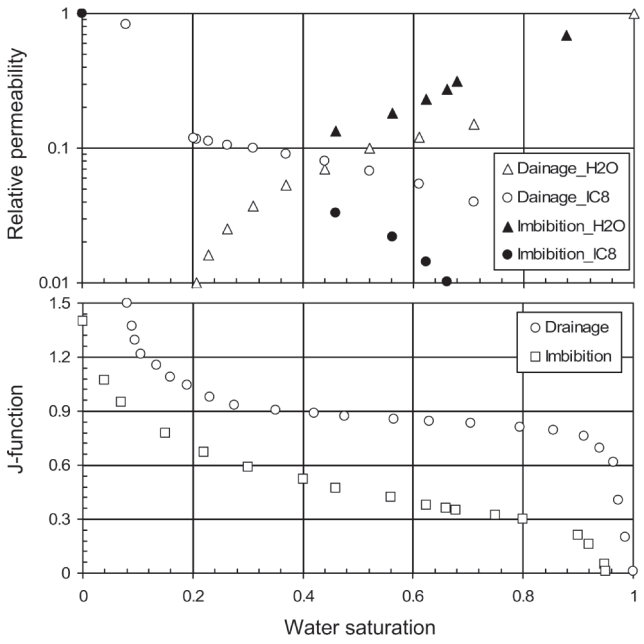

Fig. 4—Data for relative permeability and Leverett J-function in glass-bead packs.

dict the capillary and the gravity crossflow correctly, it is necessary to include these effects in the saturation equation as well. This is done by means of an operator splitting procedure. The saturation equation is first solved along the streamlines, accounting for viscous forces only. Afterward, the fluids are redistributed on the finite-difference grid with respect to the capillary and gravity forces. A more detailed description of the simulator is given by Berenblyum et al. (2003).

Results

A summary of the displacement experiments is given in **Table 3.** We isolated the effects of gravity by performing horizontal flow experiments, but included gravity in vertical and VCS experiments (see Fig. 3). The low and high IFT between fluids allowed us to study the effects of capillary forces on crossflow. We injected fluids at different flow rates to control viscous effects. The related crossflow scaling groups for all experiments were calculated using Eqs. 1 and 2. The characteristic capillary pressure difference, p_c^*, was evaluated using experimental data presented by Dawe et al. (1992) in Eq. 3. The capillary pressure data were smoothed by the van Genuchten (1980) capillary pressure model before applying the integration. Scaling groups given by Eqs. 1 and 2 are not derived to include gravity effects in vertical displacements (see Fig. 3a), because the analysis that produced the scaling groups was based on the assumption that gravity acts transverse to the average flow direction. Therefore, we did not calculate the gravity numbers for the vertical experiments.

Experimental Results and Analysis of Scaling Groups for Crossflow. Fig. 5 shows data of scaling groups for the displacements with VCS models (Experiments 14, 16, 18, and 20) that included both gravity and viscous crossflow in low-IFT, near-miscible displacements ($N_{cv}\approx 0$). The dotted lines from the y-axis show the boundaries given in Table 1. The boundary for viscous effects on the x-axis was proposed by Ekrann (1992) from simulation results. According to this plot, all low-IFT displacements with VCS models lie in the transition region, but the location changes significantly depending on the flow rate of the displacement. As a result, the effect of gravity was larger in the slower displacements.

Fig. 6 shows images taken at 0.7 PVI for different displacements with various orientations depicted in Fig. 3. In the experiment with the vertical orientation (Experiment 4), gravity acted to reduce the advance rate of the front in the high-permeability layer, because the combination of gravity and viscous forces causes

TABLE 3—SUMMARY OF THE DISPLACEMENT EXPERIMENTS

Experiment	Model	L (cm)	q (cm^3/min)	$N_{gv}M/(1+M)$	$N_{cv}M/(1+M)$	N_B
Imbibition, High-IFT Displacements (M = 0.48)						
1	Fig. 3a	33	0.57	n/a	171.0	n/a
3	Fig. 3a	33	2.31	n/a	42.1	n/a
7	Fig. 3a	33	8.45	n/a	11.5	n/a
9	Fig. 3b	36	2.20	0.0	42.3	0.0
13	Fig. 3c	36	0.60	34.0	155.0	0.22
15	Fig. 3c	36	2.13	9.6	43.7	0.22
19	Fig. 3c	36	8.53	2.4	10.9	0.22
Imbibition, Low-IFT Displacements (M = 0.41)						
2	Fig. 3a	33	0.62	n/a	0.05	n/a
4	Fig. 3a	33	2.08	n/a	0.02	n/a
8	Fig. 3a	33	8.53	n/a	0.01	n/a
10	Fig. 3b	33	2.27	0.0	0.01	0.0
14	Fig. 3c	33	0.57	4.5	0.06	75.0
16	Fig. 3c	33	2.21	1.2	0.01	120.0
20	Fig. 3c	33	8.94	0.3	0.01	30.0
Drainage, High-IFT Displacements (M = 2.08)						
5	Fig. 3a	31	2.16	n/a	68.0	n/a
11	Fig. 3b	34	1.82	0.0	89.0	0.0
17	Fig. 3c	31	2.16	8.6	68.0	0.13
Drainage, Low-IFT Displacements (M = 2.44)						
6	Fig. 3a	31	2.16	n/a	0.02	n/a
12	Fig. 3b	33	2.20	0.0	0.03	0.0
18	Fig. 3c	31	2.02	1.1	0.02	55.0

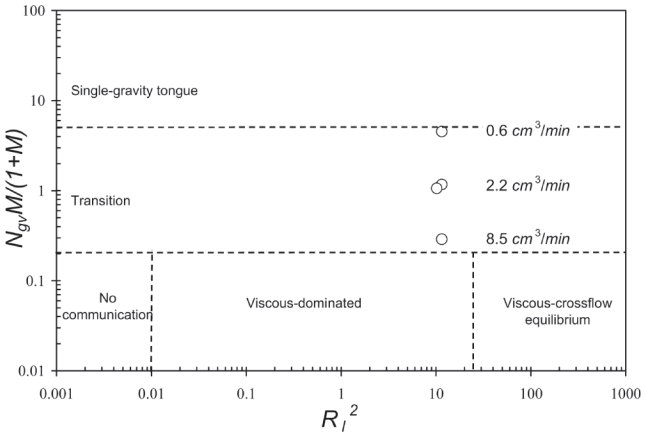

Fig. 5—Flow regions in low-IFT VCS displacements (N_{cv}≈0).

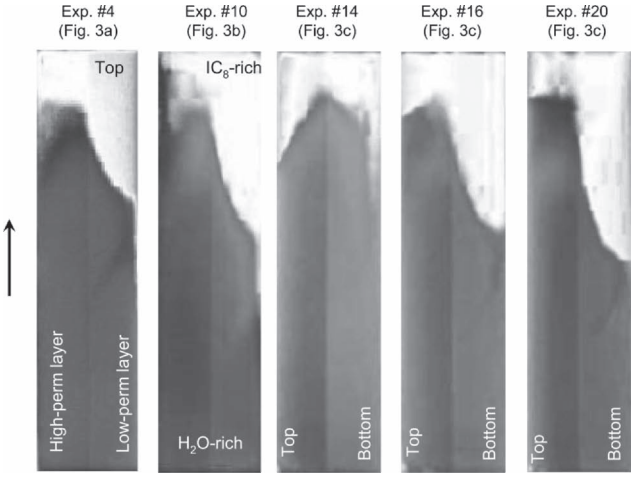

Fig. 6—Comparison of low-IFT, favorable mobility ratio displacements at PVI≈0.7.

crossflow into the low-permeability layer. Experiment 10 was performed in the horizontal orientation, with only viscous forces driving the flow (N_{gv}≈0). In that displacement, the crossflow that occurred from the high-permeability layer into the low-permeability layer was caused by the difference between layer pressures caused by the viscosity contrast. Viscous forces caused the injected fluid to flow in the high-permeability layer, resulting in viscous crossflow into the low-permeability layer, as can be seen in Fig. 6. In addition, the dye appears not to stay in the water-rich phase at the leading edge of the displacement in the high-permeability layer. We believe that this is because of sorption and/or partitioning of the dye. Comparison of the image of Experiment 4 with that of Experiment 10 also demonstrates how gravity affected that displacement.

The other three experiments were VCS displacements, which included both gravity and viscous forces. The scaling groups for those experiments shown in Table 3 and Fig. 5 suggest that the displacements were governed by a combination of viscous and gravity forces. The ratio of N_{gv} to N_{cv} (N_B) is 75, 120, and 30 for Experiments 14, 16, and 20, respectively, which also suggests that gravity forces were more important than capillary forces. In these experiments, gravity forces acted to cause injected water to crossflow from the high-permeability layer to the low-permeability layer, and, consequently, the water swept more area in the low-permeability layer than it did in the horizontal displacement (compare Experiments 10 and 16 in Fig. 6). Gravity tongues in both layers of Experiment 14 can clearly be seen in the figure. The effect of increasing displacement rate can be seen by comparing the images of Experiments 14, 16, and 20. As flow rate increased, flow occurred preferentially in the high-permeability layer, an indication that viscous forces increased compared to gravity forces. That transition is roughly consistent with the transition region suggested by Zhou et al. (1994), though it is clear that even displacement (Experiment 20) was not completely dominated by viscous forces, in which case the front in the high-permeability layer would have looked like approximately that in Experiment 10.

Fig. 7 shows the production data for the low-IFT favorable mobility ratio displacements. Although the differences are small, it is clear that the VCS experiments produced more of the IC_8-rich phase.

Fig. 8, a plot of modified capillary number vs. R_l^2, shows that high-IFT gravity-reduced immiscible displacements (Experiments 1, 3, 5, 7, 9, and 11) are in the capillary-dominated region if the scaling arguments of Zhou et al. (1994) are correct. The highest value of capillary number represents the experiment with the vertical displacement and the lowest flow rate (Experiment 1). The low-IFT displacements, on the other hand, are in the viscous-dominated regime. Higher flow rates caused the larger viscous effects. Any IFT value between 0.024 and 38.1 mN/m would bring the displacement into the capillary-viscous transition zone for the dimensions and rates of the experiments described.

Fig. 9 shows images of the high-IFT experiments performed with different orientations of the flow model. For the high-IFT displacement experiments, the water dye did not stay within the water-rich phase because of sorption and/or partitioning. Consequently, the shading of the water-rich front appears lighter than at the inlet. The displacement in the horizontal orientation (Experiment 9) included only viscous and capillary forces, but the scaling group (N_{gv}≈0, $N_{cv}M/(1+M)=42.3$) suggests that the displacement was dominated by capillary forces. The longitudinal capillary im-

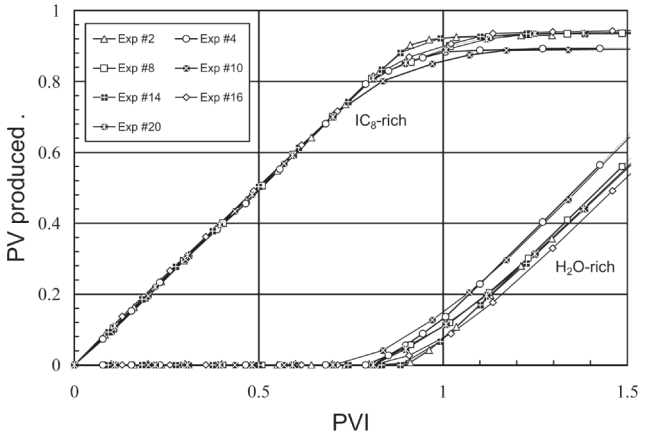

Fig. 7—Production history of low-IFT, favorable mobility ratio experiments.

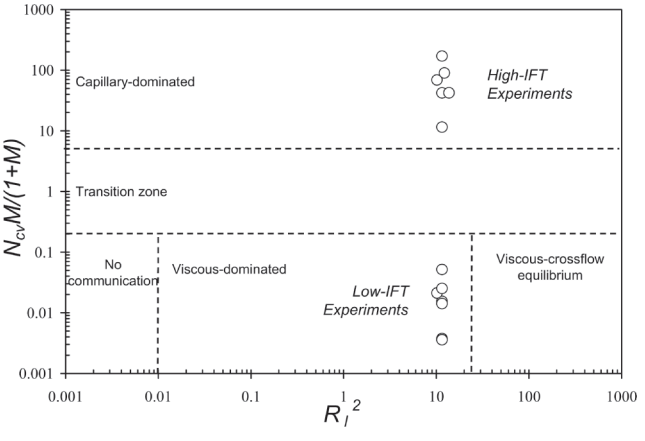

Fig. 8—Flow regions in displacements with reduced-gravity effects, N_{gv}≈0 (see Figs. 3a and 3b).

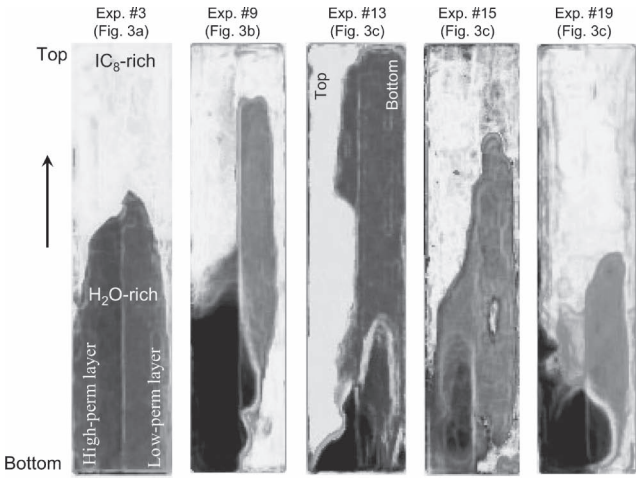

Fig. 9—Comparison of high-IFT, favorable mobility ratio displacements at PVI≈0.5.

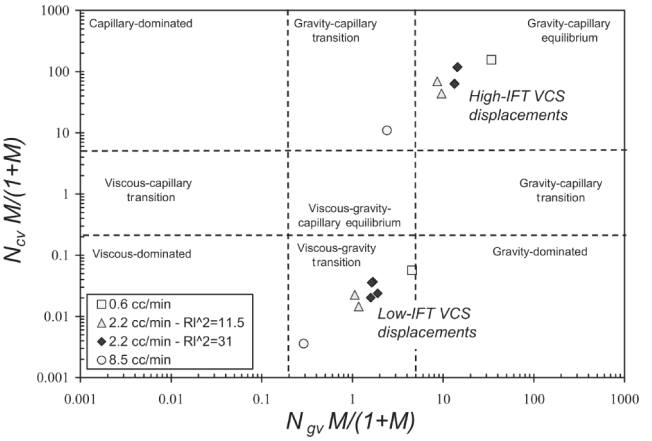

Fig. 10—Flow regions on the plot of capillary vs. gravity numbers.

bibition shown in the low-permeability layer in Experiment 9 is consistent with this argument.

The high-IFT displacements in the VCS model included all three driving forces. Comparison of the images in Fig. 9 for Experiments 13, 15, and 19 reveals the effect of changing displacement rate. As the rate increased, viscous forces caused more fluid to enter the high-permeability layer, with the result that the displacement fronts in the two layers moved at roughly equal velocity at the highest rate. This observation is also confirmed by the scaling groups for Experiments 13, 15, and 19 (see Table 3).

Fig. 10 shows a plot of modified gravity and capillary numbers for all the VCS experiments. Based on the transition values discussed previously, all three crossflow mechanisms can be clustered as shown in the figure. Note that in this version of the flow regions, there were no displacements in the capillary-dominated region. The gravity-reduced displacements found in the capillary-dominated region previously (Fig. 8) are now in the region of gravity-capillary equilibrium. Increasing flow rate shifts the displacements to the viscous-influenced regions without changing the ratio of the gravity/capillary forces.

The scaling groups for high-IFT displacements shown in Fig. 10 suggest that gravity and capillary forces influenced the flow more strongly than did viscous forces. However, the value of N_B (≈0.22 for Experiments 13, 15, and 19) for the transition region suggests that, in these displacements, capillary forces were more important than gravity forces (see Table 1). The significantly faster flow in the low-permeability layer is consistent, again, with strong capillary imbibition in the experimental images of Experiments 13, 15, and 19. It is also interesting to note that for upward flow in Experiment 3, gravity effects on the displacement were significant (compare the images of Experiments 3, 9, and 15). The scaling groups defined by Zhou et al. (1994) do not provide guidance for the effects of gravity on this kind of displacement, because the analysis that produced the scaling groups was based on the assumption that gravity acts transverse to the average flow direction. Nevertheless, it is clear that gravity acted to reduce the impact of longitudinal capillary imbibition in displacement (Experiment 3). **Fig. 11** shows the production history for the high-IFT displacements. The VCS displacement with the lowest flow rate produced less IC_8-rich phase than did other displacements. The gravity-stabilized vertical displacements gave higher recoveries than did horizontal and VCS experiments.

The scaling groups for the high-IFT, unfavorable mobility-matio drainage displacements show similar characteristics to those obtained for favorable displacements. Because the capillary pressure for flow in drainage mode was high (see the J-function in Fig. 4), the corresponding values for the scaling groups of capillary/viscous forces were also larger, as Table 3 shows. For example, Experiment 11 was a horizontal displacement with scaling groups of $N_{gv}=0$ and $N_{cv}M/(1+M)=89$ that was influenced only by the permeability differences and capillary forces. Note that the value of $N_{cv}M/(1+M)$ for the same liquid system in the same porous model was approximately half of that value for the imbibition experiment. The values of $N_{cv}M/(1+M)$ and $N_{gv}M/(1+M)$ were 68 and 8.6, respectively, for a similar experiment in the VCS orientation (Experiment 17). These values suggest that the displacement in Experiment 17 was significantly influenced by both capillary and gravity forces, with smaller effects of viscous forces. But the value of N_B for this experiment was 0.13, which is consistent with an argument that the flow was strongly affected by capillary forces. **Fig. 12** shows the images taken during the experiments. Capillary forces apparently caused the nonwetting fluid to flow in the larger pores of the high-permeability layer. A comparison of the images for Experiments 11 and 17 in Fig. 12 shows that gravity effects create a stronger tongue along the upper edge of the model (possibly induced by a combination of small local variation of pore sizes and wettability effects of the PVC sealing material near the edge of the model). The vertical displacement (Experiment 5) was still influenced by capillary forces, but gravity helped to produce more stable fronts and a larger swept area in the low-permeability layer than did other displacements. The production history for the related displacements is shown in **Fig. 13.** The gravity-stabilized experiment results in a higher recovery of the H_2O-rich phase. The recovery from the VCS experiment was slightly higher than that of the horizontal experiment. **Fig. 14** shows results of low-IFT, adverse mobility-ratio drainage experiments. In the low-IFT horizontal displacement (Experiment 12), the flow was governed primarily by viscous forces ($N_{gv}\approx 0$ and $N_{cv}M/(1+M)=0.03$). The image shown in Fig. 14 demonstrates evidence of unstable viscous flow. Scaling parameters for a similar displacement in the VCS model (Experiment 18) suggest that the VCS displacement was governed

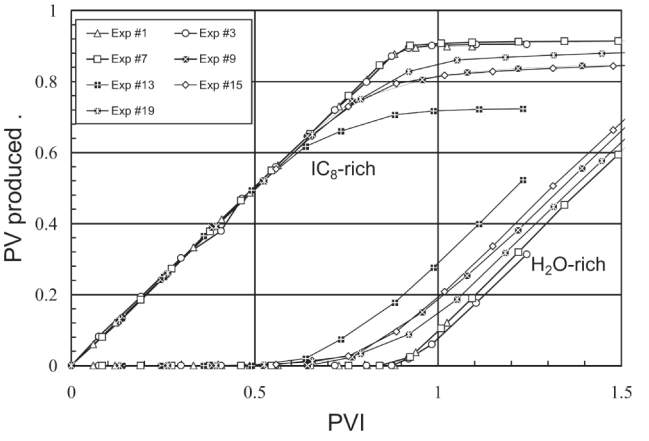

Fig. 11—Production history of high-IFT, favorable mobility ratio displacements.

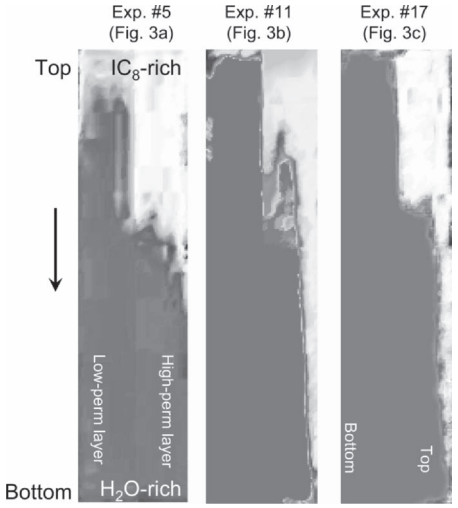

Fig. 12—Comparison of high-IFT, unfavorable mobility ratio displacements at PVI≈0.2.

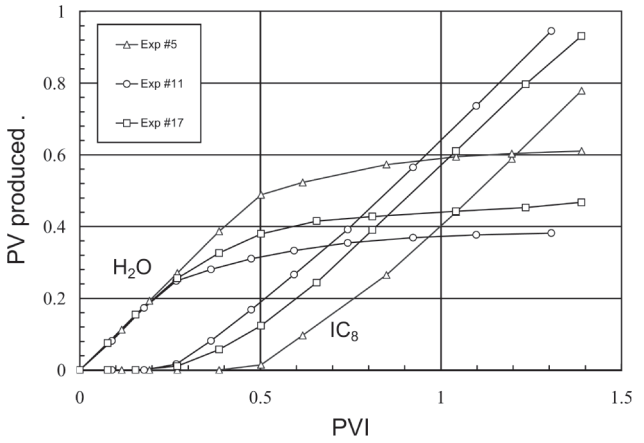

Fig. 13—Production history of high-IFT, unfavorable mobility ratio displacement experiments.

by viscous and gravity forces. The image with gravity override in Fig. 14 also supports this argument. The displacement in the vertical orientation was similar to that in the horizontal orientation. **Fig. 15** shows the production history of the low-IFT, unfavorable mobility ratio displacements. In this case, the VCS experiment gave the lowest recovery of the H_2O-rich phase. The gravity override in the VCS experiment, which can be seen in Fig. 14, caused early breakthrough and resulted in a reduction in the recovery. The other two displacements produced approximately the same amount of the displaced phase.

The combination of experimental results for low- and high-IFT displacements for imbibition and drainage experiments, and for various orientations with respect to gravity, confirm that the ranges of the scaling groups suggested by Zhou et al. (1994) are reasonable, at least for the regions where capillary or gravity forces were most important. Delineation of the details of the displacement behavior in the transition regions would require more experimental work, but it is clear that the broad outlines of the scaling analysis are consistent with the experimental observations.

Numerical Simulation Results. Eight displacements were selected for the comparison with numerical simulations. We considered first four VCS experiments representing favorable mobility-ratio imbibition and unfavorable mobility-ratio drainage processes, for both high and low IFT. Each of the experiments was simulated with the FD simulator to test whether input phase-relative permeability and capillary pressure functions (J-functions) gave reasonable predictions of displacement behavior. **Fig. 16** reports a comparison of the imbibition Experiments 15 (high IFT) and 16 (low IFT) with the equivalent numerical calculations. Fig. 16a compares the production history, while Fig. 16b shows snapshots of the fluid distributions at 0.7 PVI. The low-IFT displacement experiment and simulation agree well, but some discrepancies are seen for the high-IFT displacement. The capillary-driven imbibition in the low-permeability layer of Experiment 15 is more important in the numerical calculations. This results in a prediction of early breakthrough and a reduction in the ultimate recovery. A direct visual comparison of the fluid distributions (Fig. 16b) is made difficult by the fact that the color resulting from a mixture of dye colors (transition zones) does not scale linearly with in-situ phase saturations. In addition, the dye did not stay within its original phase for the high IFT displacement (Experiment 15). Even given these uncertainties, it is apparent that the simulations reproduce with reasonable accuracy the displacement patterns observed in the experiments.

A second set of numerical calculations for the unfavorable mobility ratio drainage processes in Experiments 17 (high IFT) and 18 (low IFT) is compared with the experimental observations in **Fig. 17.** The production histories (Fig. 17a) predicted by numerical calculations agree well with the experimental observations. However, moderate discrepancies are observed for the fluid distributions after 0.7 PVI (Fig. 17b). In particular, for the low-IFT displacement, gravity override is predicted to be more important in the numerical calculation than was observed in the experiment.

Four additional experiments were selected for comparison with FD and streamline-based simulations. For this purpose we initially

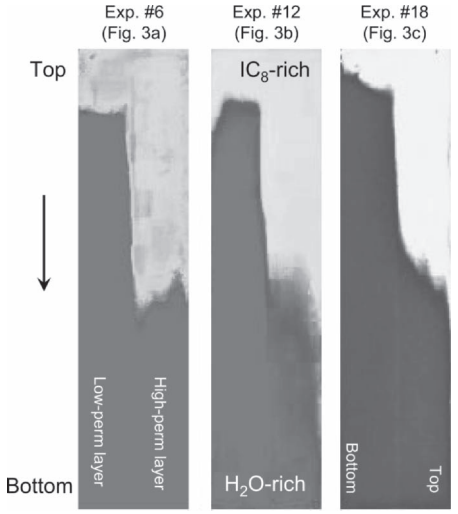

Fig. 14—Comparison of low-IFT unfavorable mobility ratio displacements at PVI≈0.2.

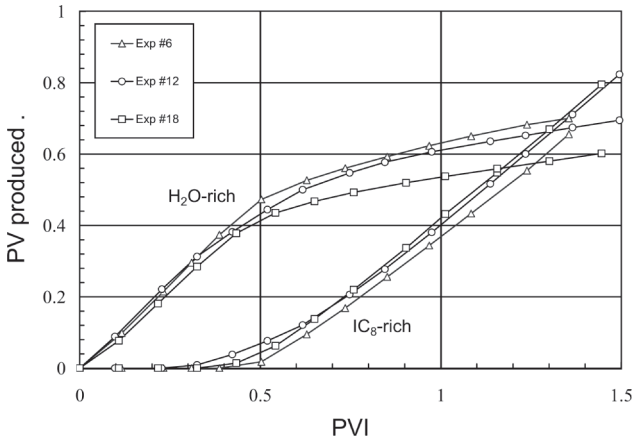

Fig. 15—Production history of low-IFT, unfavorable mobility ratio displacement experiments.

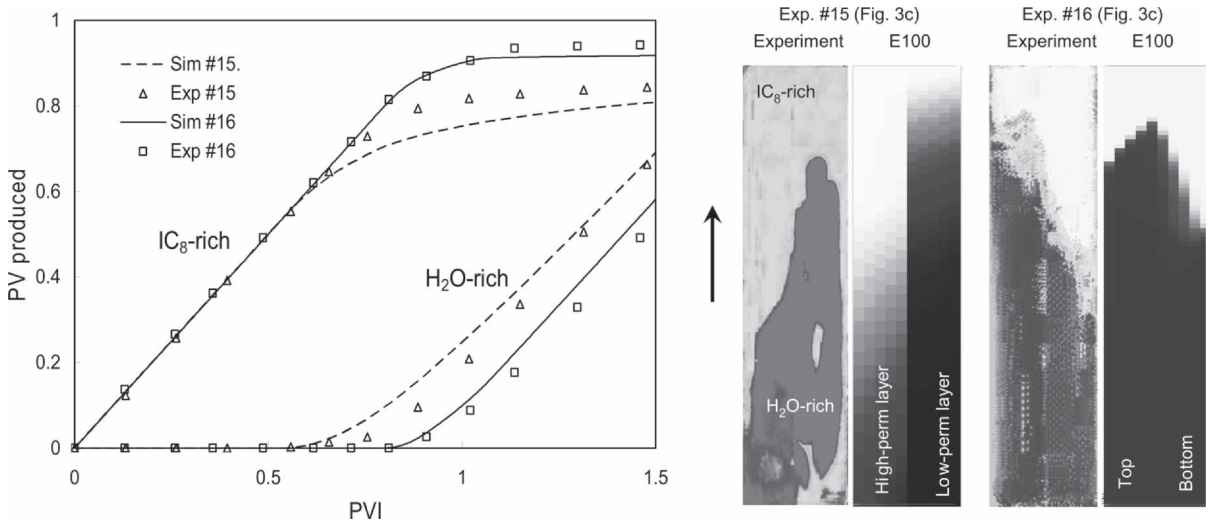

Fig. 16—(a) Comparison of production history from Experiments 15 and 16 (high- and low-IFT, favorable mobility ratio VCS displacements) and FD simulations; (b) water distribution at 0.7 PVI (color scales are different on experimental and numerical images).

consider displacement Experiment 1, a high-IFT displacement of IC_8 by H_2O in the vertical model (gravity-stabilized imbibition). **Fig. 18** summarizes the results of the displacement calculations. Fig. 18a reports the production history from the simulations, while Fig. 18b gives a snapshot of the displacement calculations at 0.65 PVI. The figure shows that both simulators predict more rapid imbibition of water into the low-permeability layer than was observed in the experiment. This, in turn, results in early breakthrough and a slightly lower predicted recovery at the point of breakthrough. Note that traditional streamline simulation, without explicit treatment of capillary effects, would predict preferential flow of water in the high-permeability layer and would not be applicable for this capillary-dominated displacement (see the next example).

In the following calculation example, we model Experiment 8: a high-rate, low-IFT, gravity-stabilized displacement in the vertical model (Fig. 3a). In this experiment, viscous and gravity forces dominate the displacement with vanishing crossflow because of capillary effects. **Fig. 19** reports (a) the production history and (b) a snapshot of the water distribution at 0.8 PVI. For this displacement, both simulation results are in excellent agreement with the experimental observations. Because the displacement in this example is dominated by viscous and gravity forces, any streamline simulator that includes gravity effects should be able to reproduce the experiment with appropriate accuracy. However, such a simulator would not be able to distinguish between Experiments 1 and 8.

Next we consider Experiment 9 (high-IFT, horizontal displacement). This experiment was dominated by capillary effects, and the propagation of water in the low-permeability layer is no longer damped by the density difference between IC_8 and H_2O. **Fig. 20** shows the production history from the FD and the streamline simulation along with the H_2O distribution after 0.5 PVI. Relative to Experiment 1, this displacement is more strongly influenced by capillary effects. Fig. 20 shows a larger discrepancy between the predicted displacement performance and the experiment for both simulation approaches. For this strongly capillary-dominated displacement, the fully implicit FD simulation predicts more accurately the fluid distributions and the timing of breakthrough. The streamline approach fails to represent an appropriate level of crossflow (overpredicts) resulting in late breakthrough, ultimate recovery that is too high, and an undesirable mass-balance error of 10%.

Finally, we consider Experiment 10. This displacement is dominated by viscous forces because of the low IFT and the horizontal orientation of the model. A comparison of the predicted

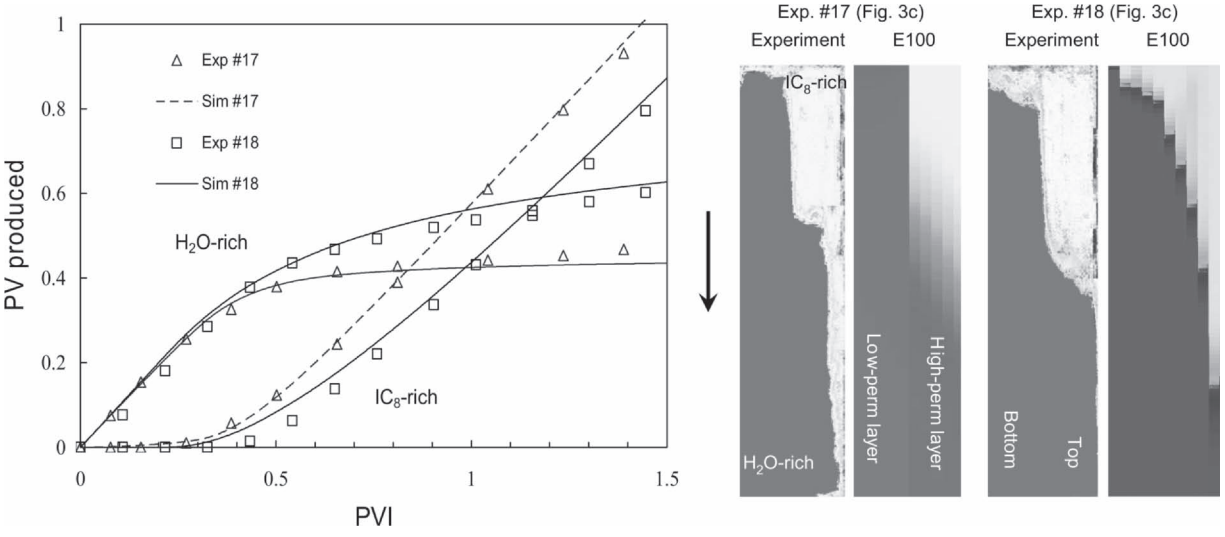

Fig. 17—(a) Comparison of production history from Experiments 17 and 18 (high- and low-IFT, favorable mobility ratio VCS displacements) and FD simulations; (b) water distribution at 0.7 PVI (color scales are different on experimental and numerical images).

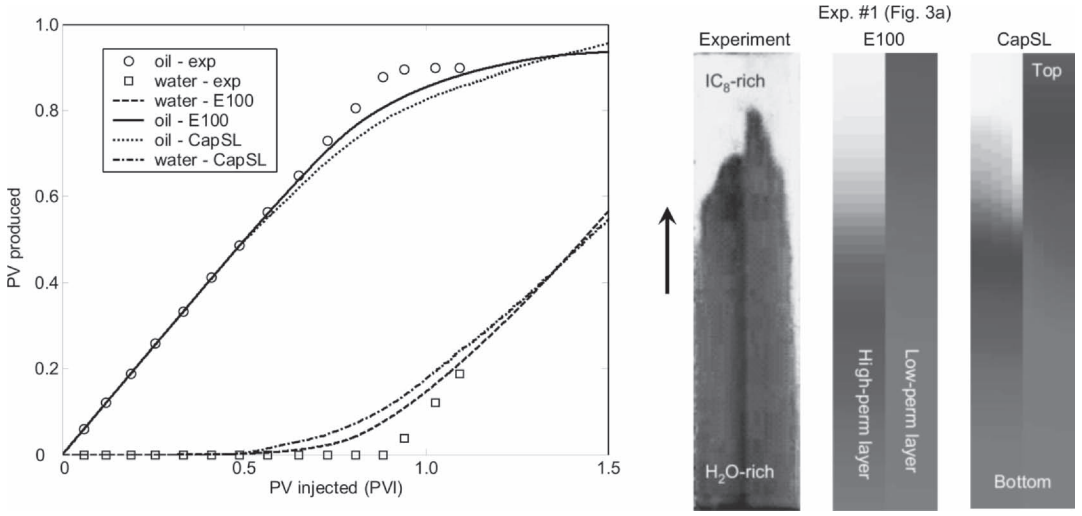

Fig. 18—(a) Production history from Experiment 1 (high-IFT, favorable mobility ratio vertical displacement) and simulations; (b) water distribution at 0.65 PVI (color scales are different on experimental and numerical images).

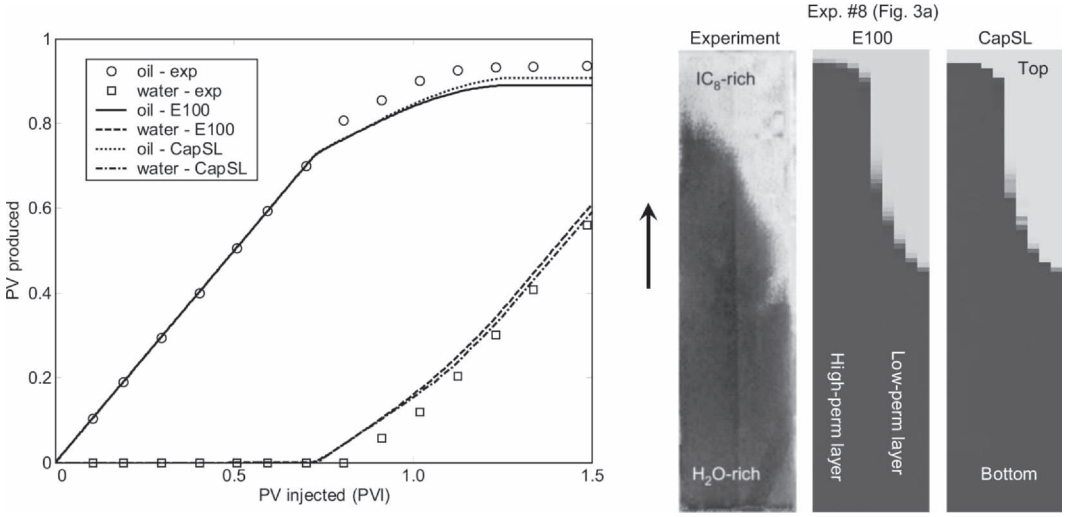

Fig. 19—(a) Production history from Experiment 8 (low-IFT, favorable mobility ratio vertical displacement) and simulations; (b) water distribution at 0.8 PVI (color scales are different on experimental and numerical images).

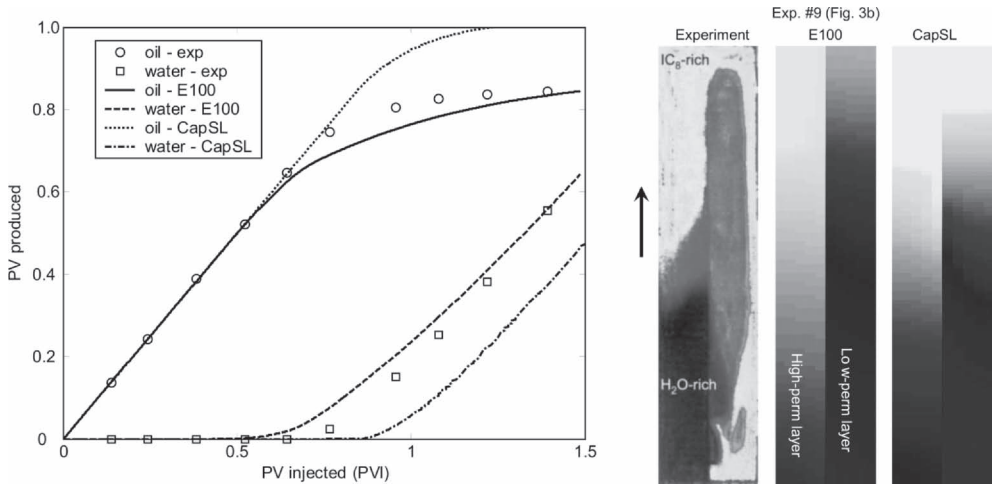

Fig. 20—(a) Production history from Experiment 9 (high-IFT, favorable mobility ratio horizontal displacement) and simulations; (b) water distribution at 0.5 PVI (color scales are different on experimental and numerical images).

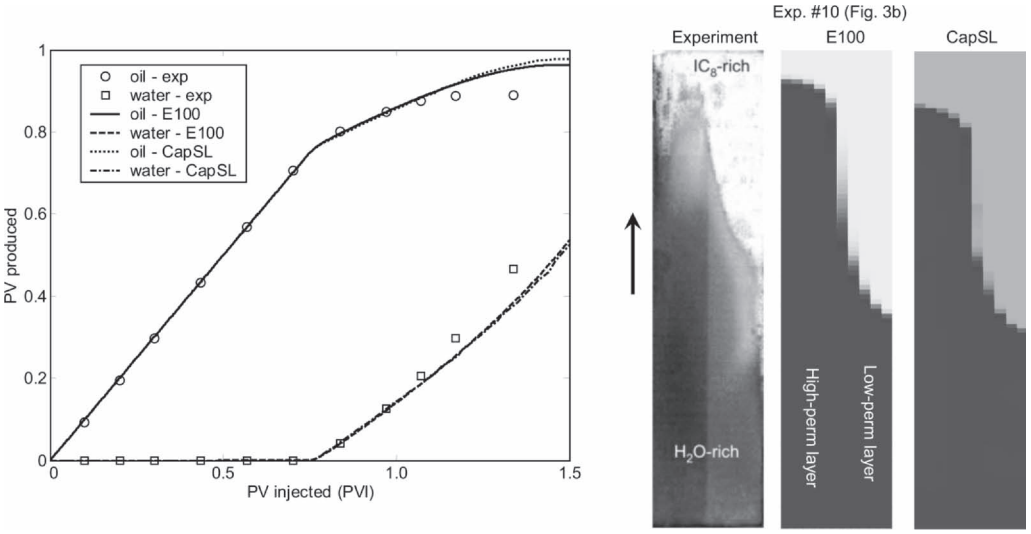

Fig. 21—(a) Production history from Experiment 10 (low-IFT, favorable mobility ratio horizontal displacement) and simulations; (b) water distribution at 0.7 PVI (color scales are different on experimental and numerical images).

production data with the experimental data is given in **Fig. 21.** The figure also shows the water distributions after 0.7 PVI. As expected, the predictions from both simulators are in excellent agreement with the experimental data for this viscous-dominated displacement.

The numerical results presented demonstrate that the fully implicit FD simulator can be applied over the full range of displacement processes with reasonable accuracy. The streamline method used in this study performed well for low to moderate capillary to viscous numbers.

Discussion

The experimental results reported demonstrate that even in very simple flow geometries and with well defined fluids with constant properties, there is a complex interplay of capillary, viscous, and gravity forces that determines overall sweep and displacement efficiency. There is, of course, little hope that experimental investigations can cover the full range of displacement conditions that will arise in field displacements. It is important, therefore, to establish that simulation tools can be used to explore the full range of the parameter space with reasonable accuracy. The simulation results presented here, though not in perfect agreement with the experiments, show the same transitions between flow regimes that were observed in the experiments. Thus, it is reasonable to use simulation to explore the interplay of capillary, viscous, and gravity forces in displacements at various scales.

The numerical results presented also demonstrate that both simulation approaches agree better with experimental observations when viscous and gravity forces are stronger than capillary forces. They also show that either the conventional FD approach or the streamline method, with appropriate representation of the effects of gravity and capillary forces, can be used to study flow behavior in many heterogeneous systems. However, for displacements that are dominated by capillary pressure, streamline simulation, even with the inclusion of a representation of capillary forces, is not the appropriate choice. In capillary-dominated flows, flow that is not aligned with streamline directions will ultimately determine the fluid distribution. For this situation, fully implicit FD methods give a more accurate representation of flow behavior.

Conclusions

A series of laboratory experiments and numerical simulations was performed to investigate the combined effects of capillary and viscous forces and gravity segregation on displacement efficiency in layered systems. The series of experiments included two-phase displacements with favorable and unfavorable mobility ratio. A wide range of capillary and gravity numbers was investigated. The combination of experimental and numerical results lead to the following conclusions:

1. Even in the simple flow geometries considered here, two-phase displacements show complex interactions of capillary, viscous, and gravity forces as the relative magnitudes of those forces are varied.
2. The boundaries of the flow regions proposed by Zhou et al. (1994) are consistent with the experimental observations reported here.
3. Finite-difference-based simulation represents the range of capillary, gravity, and viscous forces considered in this paper with reasonable accuracy, while streamline-based simulation, including capillary effects, adequately represents displacements with low to moderate capillary numbers.
4. In the transition zone where all forces play an important role in the ultimate displacement performance, the predicted flow behavior from both simulation approaches was in good enough agreement with experimental observations that it is reasonable to use these simulation approaches to explore the quantitative behavior of flows in more complex geometries.

Nomenclature

d_g = grain diameter of glass beads, L, cm
g = gravitational constant, MT^{-2}, m/s^2
H = height of porous medium, L, cm
IFT = interfacial tension, MT^{-2}, mN/m
J = Leverett J-function
k = absolute permeability, L^2, D
k_{ah} = average horizontal permeability, L^2, D
k_{av} = average vertical permeability, L^2, D
L = length of porous medium, L, cm
M = viscosity ratio
N_B = Bond number, N_{gv}/N_{cv}
N_{cv} = transverse capillary number
N_{gv} = transverse gravity number
p_c = capillary pressure, $ML^{-1}T^{-2}$, kPa
p_c^* = characteristic capillary pressure, $ML^{-1}T^{-2}$, kPa
q = flow rate, L^3T^{-1}, cm^3/min
S = saturation
S_{or} = residual oil saturation
S_w = water saturation
S_{wc} = connate water saturation
v = total velocity, LT^{-1}, cm/s
W = width of porous medium, L, cm
$\Delta\rho$ = density difference, ML^{-3}, g/cm^3

θ = contact angle, degrees
μ_o = viscosity of displaced phase, $ML^{-1}T^{-1}$, mPa·s
σ = interfacial tension, MT^{-2}, mN/m
ϕ = porosity, fraction

Acknowledgments

We gratefully acknowledge financial support from the U.S. Dept. of Energy (Contract No. DE-FC26-00BC15319) and all members of the Stanford U. Petroleum Research Inst. for Gas Injection (SUPRI-C). R. Berenblyum also acknowledges financial support from the Danish Energy Authority and affiliates of the IVC-SEP consortium.

References

Ahmed, G. 1984. An experimental study of recovery from a 2D layered sand model. MS thesis, Stanford U., Stanford, California.

Batycky, R.P. 1997. A Three-Dimensional Two-Phase Field Scale Streamline Simulator. PhD dissertation, Stanford U., Stanford, California.

Berenblyum, R.A., Shapiro, A.A., Jessen, K., Stenby, E.H., and Orr, F.M. Jr. 2003. Black Oil Streamline Simulator With Capillary Effects. Paper SPE 84037 presented at the SPE Annual Technical Conference and Exhibition, Denver, Colorado, 5–8 October.

Brock, D.C. and Orr, F.M. Jr. 1991. Flow Visualization of Viscous Fingering in Heterogeneous Porous Media. Paper SPE 22614 presented at the SPE Annual Technical Conference and Exhibition, Dallas, 6–9 October.

Burger, J.E. and Mohanty, K.K. 1997. Mass Transfer From Bypassed Zones During Gas Injection. *SPERE* **12** (2): 124–130. SPE-30768-PA.

Dawe, R.A., Wheat, M.R., and Bidner, M.S. 1992. Experimental investigation of capillary pressure effects on immiscible displacement in lensed and layered porous media. *Transport in Porous Media* **7:** 83–101.

Ekrann, S. 1992. An Analysis of Gravity-Segregated Piston-Like Displacement in Stratified Reservoirs. *SPERE* **7** (1): 143–148. SPE-18598-PA.

Fayers, J.J. and Lee, S.T. 1994. Crossflow mechanisms in oil displacement by gas drive in heterogeneous reservoirs. *In Situ* **18** (4): 369–398.

Firoozabadi, A. 1994. Miscible Displacement in Fractured Porous Media: Part I—Experiments. Paper SPE/DOE 27743 presented at the SPE/DOE Improved Oil Recovery Symposium, Tulsa, 17–20 April.

Gaucher, D.H. and Lindley, D.C. 1960. Waterflood Performance in a Stratified, Five-Spot Reservoir—A Scaled-Model Study. *Trans.,* AIME **219:** 208–215.

Jiang, Q. and Butler, R.M. 1994. Experimental studies on effects of reservoir heterogeneity on the Vapex process. *J. Canadian Pet. Tech.* **35** (10): 46–54.

Johnson, E.F., Bossler, D.P., and Naumann, V.O. 1959. Calculation of Relative Permeability From Displacement Experiments. *Trans.*, AIME **216:** 370–372.

Leverett, M.C. 1941. Capillary Behavior in Porous Media. *Trans.*, AIME **142:** 152–169. SPE-1223-PA.

Mohanty, K.K. and Johnson, S.W. 1993. Interpretation of Laboratory Gasfloods With Multidimensional Compositional Modeling. *SPERE* **8** (1): 59–66. SPE-21204-PA.

Morrow, N.R.: 1976. Capillary Pressure Correlations for Uniformly Wetted Porous Media. *Journal of Canadian Petroleum Technology*. **15** (4): 49–69.

Orr, F.M. Jr. 2004. High Resolution Prediction of Gas Injection Process Performance for Heterogeneous Reservoirs. Final Report for DOE Project, DE-FC26-00BC15319, Stanford U., Stanford, California.

Peters, B.M., Zhou, D., and Blunt, M.J. 1998. Experimental Investigation of Scaling Factors That Describe Miscible Floods in Layered Systems. Paper SPE/DOE 39624 presented at the SPE/DOE Improved Oil Recovery Symposium, Tulsa, 19–22 April.

Richardson, J.G. and Perkins, F.M. Jr. 1957. A Laboratory Investigation of the Effect of the Rate on Recovery of Oil by Waterflooding. *Trans.,* AIME **210:** 114–121.

Schechter, D.S., Zhou, D., and Orr, F.M. Jr. 1994. Low IFT drainage and imbibition. *J. Pet. Sci. Eng.* **11:** 283–300.

Shook, M., Li, D., and Lake, L.W. 1992. Scaling immiscible flow through permeable media by inspectional analysis. *In Situ* **16** (4): 311.

Tchelepi, H.A. 1994. Viscous fingering, gravity segregation and permeability heterogeneity in two-dimensional and three-dimensional flows. PhD dissertation, Stanford U., Stanford, California.

van Genuchten, M.T. 1980. A closed-form equation for predicting the hydraulic conductivity of unsaturated soils. *Sol. Sci. Soc. Am. J.* **44:** 892–898.

Wylie, P. and Mohanty, K.K. 1997. Effect of Water Saturation on Oil Recovery by Near-Miscible Gas Injection. *SPERE* **12** (4): 264–268. SPE-36718-PA.

Zapata, V.J. and Lake, L.W. 1981. A Theoretical Analysis of Viscous Crossflow. Paper SPE 10111 presented at the SPE Annual Technical Conference and Exhibition, San Antonio, Texas, 4–7 October.

Zhou, D., Fayers, F.J., and Orr, F.M. Jr. 1994. Scaling of Multiphase Flow in Simple Heterogeneous Porous Media. Paper SPE/DOE 27833 presented at the SPE/DOE Improved Oil Recovery Symposium, Tulsa, 17–20 April.

SI Metric Conversion Factors

bbl × 1.589 873	E–01 = m^3
cp × 1.0*	E–03 = Pa·s
ft × 3.048*	E–01 = m
ft^3 × 2.831 685	E–02 = m^3
ft^3/s × 2.831 685	E+01 = cm^3/s
in. × 2.54*	E+00 = cm
lbf × 4.448 222	E+00 = N
lbm/ft^3 × 1.601 850	E–02 = g/cm^3
md × 9.869 233	E–04 = mm^2
psi × 6.894 757	E+00 = kPa

* Conversion factor is exact.

Yildiray Cinar is a lecturer in the School of Petroleum Engineering at the U. of New South Wales (UNSW). Previously, he held various research positions at Stanford U., Clausthal Technical U., and Istanbul Technical U. He holds BS and MS degrees from Istanbul Technical U. and a Dr.-Ing. degree from Clausthal Technical U., all in petroleum engineering. He is the faculty sponsor of the SPE Student Chapter at UNSW. **Kristian Jessen** is an acting assistant professor in the Dept. of Petroleum Engineering at Stanford U. He is a co-founder of the company Tie-Line Technology, specializing in software/algorithms for modeling-phase behavior and miscibility in relation to EOR. He holds a BS degree from the Danish Engineering Academy and MS and PhD degrees from the Technical U. of Denmark, all in chemical engineering. **Roman Berenblyum** is a reservoir engineer at Rogaland Research Center. Previously, he was a reservoir engineer at JSC Petroleum Technologies. He holds a BS degree from Mendelev U. of Chemical Technology of Russia and a PhD degree from the Technical U. of Denmark, both in chemical engineering. **Ruben Juanes** is an assistant professor in the Dept. of Petroleum Engineering at the U. of Texas at Austin. Previously, he was an acting professor at Stanford U. and an assistant professor at the U. of La Coruña. His current interests include the simulation of coupled reservoir geomechanics and fluid flow, multiscale numerical methods, and three-phase flow theory. Juanes holds MS and PhD degrees in civil and environmental engineering from the U. of California at Berkeley. **Franklin M. Orr Jr.** is the Beal Professor of Petroleum Engineering and Director of the Global Climate and Energy Project at Stanford U. He served as Dean, School of Earth Sciences, at Stanford from 1994–2002. Previously, he was head of the miscible flooding section at the New Mexico Petroleum Recovery Research Center and adjunct associate professor of petroleum engineering at the New Mexico Inst. of Mining and Technology. Before that, he was a research engineer at the Shell Development Co., Bellaire Research Center. He holds a BS degree from Stanford U. and a PhD degree from the U. of Minnesota, both in chemical engineering.